Rare Metal Materials and Engineering
Volume 54, Issue 11, November 2025
Available online at www.rmme.ac.cn

Science Press

Cite this article as: Li Chunjian, Xu Kai, Feng Wei, et al. Effect of Rare Earth on Microstructure and Properties of Deposited Metal in Submerged Arc Welding of 1000 MPa Grade High-Strength Steel[J]. Rare Metal Materials and Engineering, 2025, 54(11): 2729-2738. DOI: https://doi.org/10.12442/j.issn.1002-185X.E20240568.

ARTICLE

Effect of Rare Earth on Microstructure and Properties of Deposited Metal in Submerged Arc Welding of 1000 MPa Grade High-Strength Steel

Li Chunjian[1,2], Xu Kai[1,2], Feng Wei[1], Song Changhong[1], Zhang Qingsu[1], Hao Qianyu[1], Zheng Yongqiang[1], Guo Xuchao[3]

[1] Harbin Well Welding Co., Ltd, Harbin 150000, China; [2] Harbin Welding Institute Co., Ltd, China Academy of Machinery Science and Technology Group Co., Ltd, Harbin 150028, China; [3] Suzhou Space Pioneer Co., Ltd, Suzhou 215004 China

Abstract: The optimization of deposited metal properties through the addition of rare earth elements to welding materials was explored. Utilizing optical microscope, scanning electron microscope, energy dispersive spectroscope, and X-ray diffractometer, combined with software tools like Matlab, Image-Pro Plus, and CHANNEL5, the influence mechanism of rare earth element addition on the strength, toughness, and inclusions of deposited metal in 1000 MPa grade high-strength steel was investigated. The results indicate that the incorporation of rare earth elements enhances the weldability of the welding materials. With the addition of rare earth elements, the tensile strength of the deposited metal increases from 935 MPa to 960 MPa. However, further addition leads to a decrease in tensile strength, while the yield strength continuously increases by 8.5%–17.2%. The addition of appropriate amounts of rare earth elements results in an increase in acicular ferrite and retained austenite content, as well as grain refinement in the deposited metal, leading to 8.5%–24.3% and 15.6%–42.2% enhancement in impact energy at −40 °C and −60 °C, respectively. Additionally, the proper addition of rare earth elements modifies the inclusions and generates fine and dispersed composite inclusions that bond better with the matrix, thereby optimizing the properties of the deposited metal through various mechanisms. Adding an appropriate amount of rare earth elements can significantly enhance the properties of the deposited metal in 1000 MPa grade high-strength steel, and improve the match between high strength and toughness, meeting the demands for high-strength steel used in hydropower applications.

Key words: 1000 MPa grade high-strength steel; deposited metal; submerged arc welding; rare earth element; inclusions

1 Introduction

Hydropower possesses characteristics such as strong environmental friendliness, significant economic benefits, outstanding social comprehensive benefits, stable and secure energy supply, mature and reliable technique, and also makes important contribution to ecological and environmental protection. It has played a crucial role in promoting green economic development. To enhance the capacity of hydroelectric generation, hydropower institutions worldwide have continuously increased the rotation speed, efficiency, and capacity of generator sets. This, in turn, has raised higher requirements for the performance of steel used in penstocks, fins, branch pipes, spiral cases, and other components in hydropower stations[1–2]. In order to meet the layout of hydropower stations, reduce the mass and wall thickness of penstocks and spiral cases, improve the welding performance of welded joints, and lower overall project costs, the construction of hydropower stations has progressively adopted higher strength grade steels, advancing from the early 500 MPa grade to the 1000 MPa grade. Japan has already applied 1000 MPa grade high-strength steel in the Kanagawa hydropower station, significantly enhancing equipment stability and reducing construction costs[3–4]. However, its

Received date: November 25, 2024
Foundation item: Provincial Key Research and Development Plan of Heilongjiang (2022ZX04A01)
Corresponding author: Xu Kai, Ph. D., Professor, Harbin Welding Institute Co., Ltd, China Academy of Machinery Science and Technology Group Co., Ltd, Harbin 150028, P. R. China, Tel: 0086-451-86333949, E-mail: xkwelding@163.com

application in hydropower facilities in China is relatively restricted, indicating a significant gap compared to countries that have mastered this technology. To address this problem, Baotou Groups in China developed the 1000 MPa grade steel for hydropower use and achieved mass production across various thicknesses. Nevertheless, there is a paucity of research on corresponding welding materials. And the match between high strength and toughness in deposited metal remains a challenge in welding material development.

Rare earth elements (REEs), as important additives in the metallurgical industry, exhibit great potential in improving the microstructure and comprehensive properties of steel materials due to their unique physicochemical properties. Since the high-alloy stainless steel produced by Carpenter Company and the steel casting manufactured by American Steel Foundries in the early 1950s, REEs have attracted considerable interest worldwide[5–6]. In recent years, numerous reports have documented the application of REEs in high strength low alloy (HSLA) steel to enhance their toughness[7–11], and research on improving weldability has also been reported. For instance, Baotou Groups used REEs in Q690CF to reduce carbon equivalent and welding crack sensitivity index, thereby enhancing the weldability of HSLA steel[12]. However, the application of REEs in welding materials for 1000 MPa grade high-strength steel is rarely explored, and systematic research on the microstructure and properties of deposited metal by submerged arc welding is scarce.

Therefore, this study aims to optimize the submerged arc welding materials for 1000 MPa grade high-strength steel using REEs. Through performance tests, microstructural observations, and statistical analysis of inclusions, the influence mechanisms of REEs on the strength, toughness, and inclusions of deposited metal were investigated using optical microscope (OM), scanning electron microscope (SEM), and electron backscatter diffractometer (EBSD). This research provides support for both research and practical engineering applications of deposited metal.

2 Experiment

The test steel plate was made of Q235 material, with dimensions of 350 mm×300 mm×20 mm. A 45° V-shaped groove was cut, and the bottom gap of test plate was set to 16 mm. A backing plate of 350 mm×30 mm×10 mm was placed at the bottom of test plate. The base welding was performed using J107S, a 1000 MPa grade high-strength steel electrode produced by Harbin Well Welding Co., Ltd. A 4 mm transition layer was deposited on the surface of the groove. The schematic diagram of the welded test plate is shown in Fig.1. The welding process parameters are presented in Table 1. Through experiments, these parameters are found to be the optimal process parameters[13].

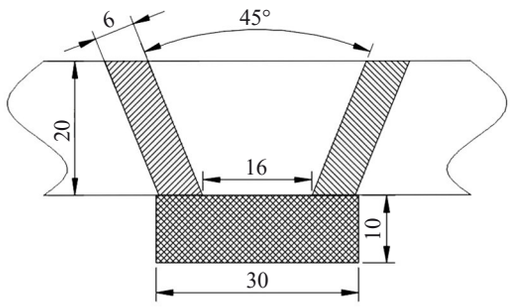

Fig.1 Schematic diagram of welded test plate

For the welding material, the self-developed 1000 MPa grade high-strength steel submerged arc welding wire HW-100S was used to weld the test plate. The welding wire has a diameter of *Φ*3.2 mm. Following the design concepts of purification and low carbonization, it has low content of P and S, and incorporated elements such as Cr, Ni, Si, Mn, Ti, and Mo, meeting the requirements for matching high strength and toughness of the deposited metal. The composition of the used welding wire is shown in Table 2.

The used welding flux was a fluoride-alkali type, with strict control over elements such as P, S, and O in the deposited metal. In the composition of the flux, CaF_2 plays a key role in slag formation. It effectively reduces the melting point, viscosity, and surface tension of the slag, enhancing its fluidity and reducing gaseous impurities in the weld metal. This aids in the release of gas from the weld and has a certain dehydrogenation effect, reducing the diffusible hydrogen content in the weld[14]. MgO increases the alkalinity of the flux, thereby enhancing the impact toughness of the weld metal and significantly affecting the welding process performance[15]. SiO_2 reduces the alkalinity of the flux and synergistically works with CaF_2 to influence the resistance of flux to porosity and corrosion. The acicular and fibrous crystal morphology of wollastonite in the flux increases particle strength and reduces particle fragmentation[16]. Al_2O_3 can increase the surface tension of the molten slag and is an adjuster for slag viscosity and flux alkalinity[17]. CaO is a major component of the molten slag. It regulates the alkalinity of the slag and effectively enhances the ability of flux to withstand high currents, improving the surface tension and interfacial tension of the molten slag[18]. TiO_2 improves the viscosity and interfacial tension of the molten slag, promoting the discharge of the slag system during welding[19]. MnO combines with SiO_2 during welding to form complex silicates, generating good weld slag to protect the weld from the influence of N and O in the air. The reduced element Mn enhances the strength and impact toughness of the weld, and combines with S in the weld to form MnS, which acts as a

Table 1 Welding process parameters

Welding current, *I*/A	Arc voltage, *U*/V	Welding speed, *v*/cm·min^{-1}	Interlayer temperature, T_0/°C	Post-heating temperature, T_1/°C
450	32	40	≤200	350

Table 2 Composition of 1000 MPa grade high-strength steel welding wire (wt%)

C	Si	Mn	S	P	Cr	Ni	Mo	Fe
0.12	0.18	1.98	0.003	0.007	0.55	2.78	0.45	Bal.

desulfurizer, thereby reducing the tendency for hot cracking. To facilitate the rapid escape of gas during welding, ensure welding process performance, and obtain a weld with a smooth and aesthetically pleasing surface, the flux particle size is set to 250–1700 μm. In summary, the main components of the flux are shown in Table 3. REEs were introduced into the deposited metal by adding rare earth fluorides of 380 μm with a purity greater than 99.95% to the flux. The designed REEs addition amounts are shown in Table 4.

The welded plate was sampled according to the method shown in Fig. 2. Tensile test specimens were prepared in accordance with the standard GB/T 228.1-2021 of *Metallic Materials-Tensile Testing-Part 1: Method of Test at Room Temperature* and tested on a UTM5305SYXL electronic tensile testing machine. Impact test specimens for temperatures of −40 °C and −60 °C were prepared in accordance with the standard GB/T 229-2020 of *Metallic Materials-Charpy Pendulum Impact Test Method*, with three specimens prepared for each temperature. These specimens were tested on a JBN-300B impact testing machine using the Charpy V-notch impact test method. In accordance with the standard GB/T 223.92-2023 of *Determination of Lanthanum, Cerium, Praseodymium, Neodymium, and Samarium Content-Inductively Coupled Plasma Mass Spectrometry Method*, deposited metal powder was drilled from a depth of 1/2 of the weld bead. The powder and the rare earth components in the prepared flux were analyzed using inductively coupled plasma-mass spectrometer (ICP-MS) on an ICAP6300 Radial

Table 3 Composition of 1000 MPa grade high-strength steel welding flux (wt%)

CaF_2	SiO_2	MgO	TiO_2	Al_2O_3	CaO
20–28	5–8	18–21	5–8	16–24	16–22

Table 4 Designed addition amounts of REEs to welding flux

Specimen	1	2	3	4
Addition amount/parts	0	1	2	4

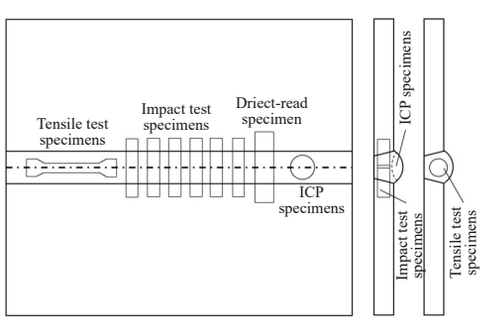

Fig.2 Schematic diagram of sampling locations

instrument. The direct-read specimen was processed into a metallographic specimen through wire cutting and hot mounting. After grinding and polishing, 100 images were randomly taken at 1000× magnification using OM (OLYMPUSGX51). The inclusions were analyzed using Image-Pro Plus software. The metallographic specimen was then chemically etched with a 2.5% nitric acid alcohol solution and observed under OM to examine the metallographic microstructure of the deposited metal. The fracture morphology and high-magnification metallographic microstructure of specimens in the low-temperature impact test at −60 °C were observed using SEM (Hitachi SU5000). For EBSD specimens, after grinding and polishing, electrolytic polishing was performed using a solution consisting of 10% perchloric acid+90% glacial acetic acid. The specimens were then observed using SEM with a scanning step size of 0.1 μm. After polishing, the specimen was analyzed for phase composition using XRD (X' Pert PRO) with a Cu target and a scanning rate of 2°/min.

3 Results and Discussion

3.1 Weldability and mechanical properties

The macroscopic morphologies of the deposited metal weld beads are shown in Fig. 3, where Fig. 3a – 3d correspond to specimens 1–4, respectively, and the welding process properties are presented in Table 5. Before and after the addition of REEs, the welding materials both exhibit excellent processability, with no splash during the welding process. The deposited metal is straight and smooth, without defects such as undercut, slag inclusion, or pits. The mechanical properties of the deposited metal by the submerged arc welding of 1000 MPa grade high-strength steel with different rare earth contents are shown in Table 6, and the strength-toughness relationship of the deposited metal is illustrated in Fig. 4. When the REEs addition was 1 part, there is no significant change in tensile strength, which remains around 930 MPa. Upon further increasing the REEs addition to 2 parts, the

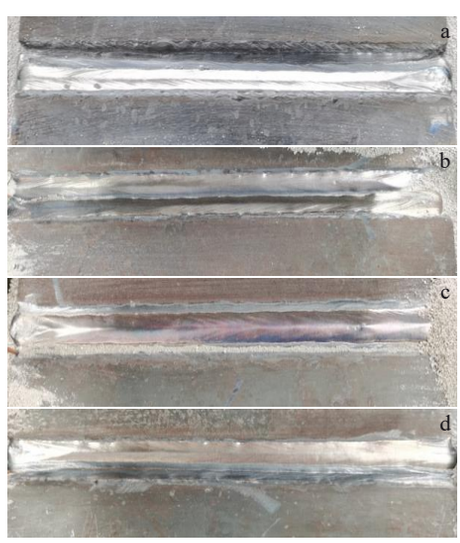

Fig.3 Macroscopic morphologies of deposited metal weld bead: (a) specimen 1; (2) specimen 2; (3) specimen 3; (4) specimen 4

Table 5 Welding process characteristics of specimens

Specimen	Welding process properties
1	During the welding process, there is no spatter, the slag removal effect is good, and there are no defects such as undercut, slag inclusion, or pits.
2	During the welding process, there is no spatter, the slag removal effect is good, and there are no defects such as undercut, slag inclusion, or pits.
3	The slag removal is favorable, the slag shell is intact, and the oxidation color is relatively heavy.
4	The slag removal for the first two layers is poor, but it improves as the number of layers increases, and the oxidation color is relatively heavy.

Table 6 Mechanical properties of deposited metal with different REEs contents

Specimen	Tensile strength, R_m/MPa	Yield strength, $R_{p0.2}$/MPa	Elongation, A/%	Impact energy at −40 °C, A_{KV2}/J			Impact energy at −60 °C, A_{KV2}/J		
1	935	740	16.0	87	86	86	53	59	61
2	930	820	19.0	103	106	89	81	82	82
3	960	867	15.5	86	104	93	74	80	78
4	885	803	18.5	85	81	71	72	69	73

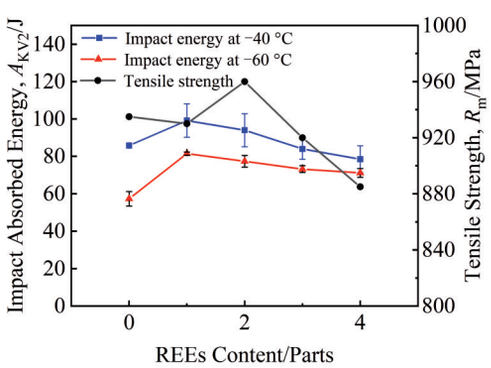

Fig.4 Tensile strength and toughness of deposited metal with different REEs contents

yield strength increases from 740 MPa to 820 MPa, representing an increase of 10.8%; the tensile strength and yield strength increase by 2.7% and 17.2%, respectively. When the addition amount reaches 4 parts, the tensile strength decreases by 5.3%, but the yield strength still increases by 8.5%, compared to the unadded case. The low-temperature toughness of the 1000 MPa grade high-strength steel deposited metal is overall enhanced after adding REEs for treatment, but the increase first rises and then declines, with an 8.5% to 24.3% increase in impact energy at −40 °C and a 15.6% to 42.2% increase at −60 °C. Therefore, the mechanical test results indicate that REEs can significantly increase the yield strength, lower the ductile-to-brittle transition temperature of the deposited metal, and enhance the overall toughness. The optimal REEs addition is 2 parts, which ensures a good strength-toughness match. With a tensile strength of 950 MPa meeting engineering requirements, the impact absorption energy at −60 °C reaches over 75 J, far exceeding engineering specifications.

3.2 Chemical testing

The ICP testing of the deposited metal and the direct-read results are shown in Table 7. It can be observed that most alloy elements do not change significantly after the addition of REEs, the sulfur (S) content increases slightly, and there is no significant change in oxygen (O). Some scholars[20] have proposed through thermodynamic calculations that REEs have a greater affinity for O than S, and will preferentially combine with O to form inclusions, which can weaken the desulfurization effect. During the welding process of specimen 3, a relatively sufficient metallurgical reaction occurs between the REEs and O, resulting in a heavier oxidation color on the weld bead. Chemical testing also shows a higher content of element S, which affects the corrosion resistance of the specimen and prolongs the corrosion time during the preparation of metallographic specimens by 20%. From the ICP testing results, it can be found that the proportion of REEs present in the deposited metal is the same as the added amount, indicating that the transition of REEs is relatively stable. However, to achieve better improvement effects of mechanical properties, it is necessary to adjust the

Table 7 Direct-read results of ICP testing of deposited metal (wt%)

Specimen	C	Si	Mn	P	S	Cr	Ni	Mo	O	Re
1	0.078	0.17	1.80	0.010	0.002 3	0.41	2.64	0.69	0.03	0
2	0.075	0.14	1.87	0.012	0.003 0	0.46	2.81	0.75	0.03	0.000 076
3	0.086	0.14	1.82	0.012	0.003 6	0.44	2.75	0.68	0.03	0.000 12
4	0.073	0.12	1.86	0.012	0.003 1	0.45	2.85	0.77	0.03	0.000 25

process parameters to increase the transition coefficient.

3.3 Microstructure of deposited metal

The microstructure of the deposited metal is depicted in Fig.5. Through a comparative analysis of the microstructures, it is evident that REEs do not significantly alter the microstructural composition of 1000 MPa grade HSLA steel, which consists of ferrite (F), bainite (B), and martensite-austenite (M-A) constituents. F includes blocky proeutectoid ferrite (PF) and acicular ferrite (AF). The AF, benefiting from its interlocking structure, effectively impedes crack propagation. Additionally, AF can completely encapsulate particles of non-metallic inclusions traditionally regarded as harmful, thereby significantly reducing or even eliminating the detrimental effects of these inclusions on the plasticity and toughness of material. Increasing the proportion of AF is a key method for enhancing the toughness. As observed in Fig. 5a and 5d, the number of AF significantly increases, and the size of blocky ferrite decreases after the addition of REEs, explaining the enhanced low-temperature impact toughness. According to Fig. 5b and 5e, there are numerous fine and dispersed M-A constituents in the microstructure, which can hinder dislocation movement and reduce stress concentration, thus impeding crack propagation. The impact fracture morphologies of the deposited metal are shown in Fig.5c and 5f. It can be seen that both fracture modes exhibit microporous aggregation type ductile fractures. A few tear ridges can be found in specimen 1, while specimen 3 displays deeper and denser dimples, indicating superior toughness.

The microstructure of the deposited metal of 1000 MPa grade high-strength steel with 0, 2, and 4 parts of REEs addition was analyzed using EBSD. The grain orientation is shown in Fig.6. The scanning location is at the intersection of two weld beads in the weld center. It can be observed that the grains exhibit a typical columnar structure. The grain orientation in specimens 1 and 4 is more pronounced in certain regions, while the orientation in specimen 3 is relatively random. Analysis of the grain boundaries and grains using CHANNEL5 reveals that the proportion of low-angle grain boundaries (2°–15°) is 27% for all three specimens, and the proportion of high-anglegrain boundaries (>15°) is 73%, with the majority distributed between 50°–60°, accounting for 62%. The average grain sizes of specimens 1, 3, and 4 are 1.60, 1.41, and 1.87 μm, and the average grain areas are 3.99, 2.82, and 4.93 μm^2, respectively. The proportion of grains with various sizes is shown in Fig.7. It can be seen that after appropriate REEs treatment of 1000 MPa grade high-strength steel, the proportion of grains smaller than 1 μm increases significantly from 33% to 45%, while the proportion of grains between 1–3 μm decreases. Combined with Fig.6, it can be inferred that the grain size is more uniform and the distribution is more reasonable. However, excessive REEs addition leads to coarse grains and an increase in large-sized grains, resulting in an initial increase and a subsequent decrease in tensile strength. Nonetheless, specimen 4 still exhibits a reduction in proportion of grains within the size range of 1–3 μm, possesses a relatively smaller average grain size, and contains a large number of high-angle grain boundaries. During crack propagation, these features cause crack deflection and blunting, hindering rapid crack propagation. Therefore, specimen 4 retains good low-temperature impact toughness.

Using EBSD phase distinction function to analyze the 1000 MPa grade high-strength steel deposited metals before and after adding REEs, and combining with XRD analysis results in Fig.8 and the microstructure morphologies shown in Fig.9, it can be observed that the retained austenite is distributed in a diffused and dot-like manner along the dendrite and grain boundaries. The proportions of retained austenite structures of specimens 1, 3, and 4 are 0.25%, 0.51%, and 0.41%, respectively. Ref. [21–22] indicate that REEs tend to segregate

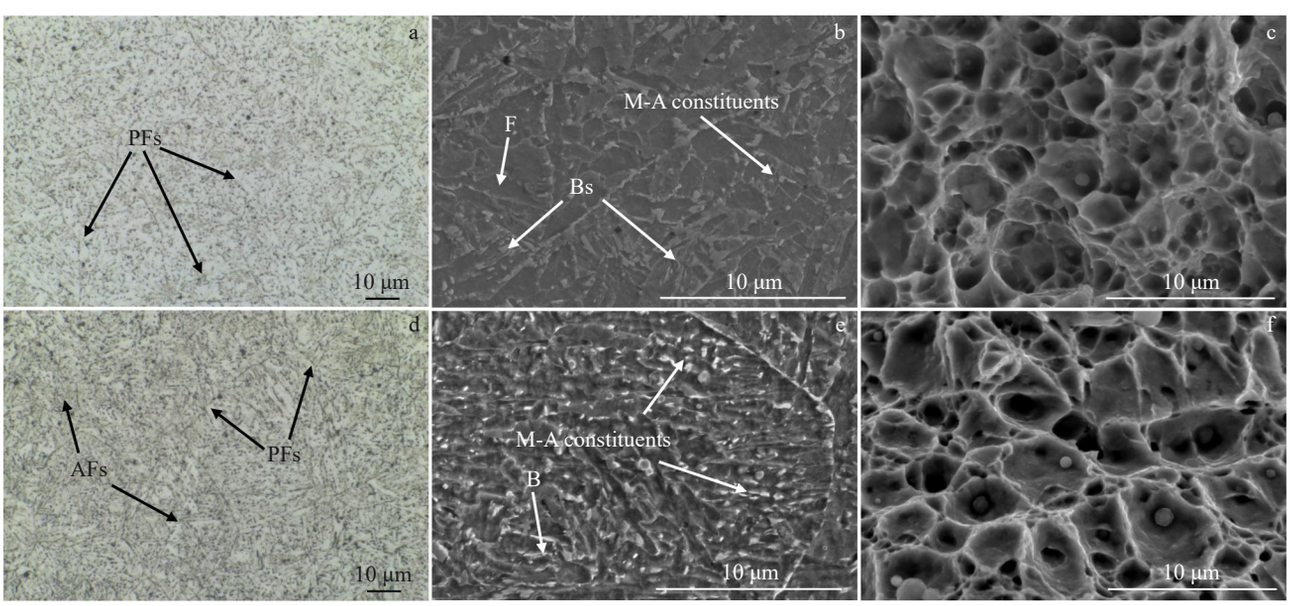

Fig.5 Microstructures of deposited metal of specimen 1 (a–c) and specimen 3 (d–f)

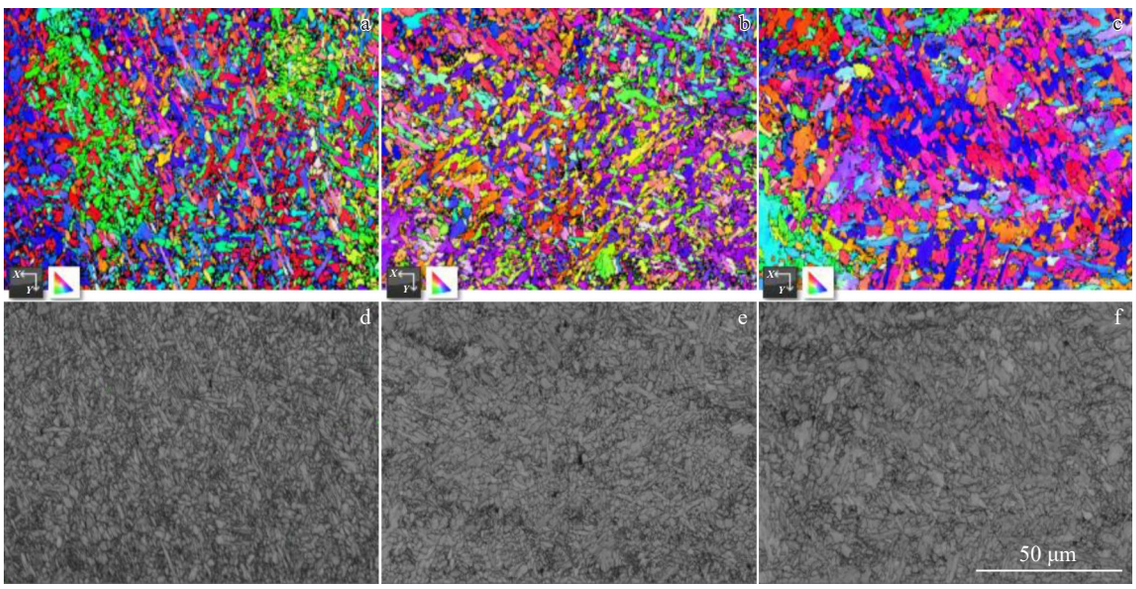

Fig.6 EBSD grain orientation images (a–c) and grain boundary images (d–f) of deposited metal of specimen 1 (a, d), specimen 3 (b, e), and specimen 4 (c, f)

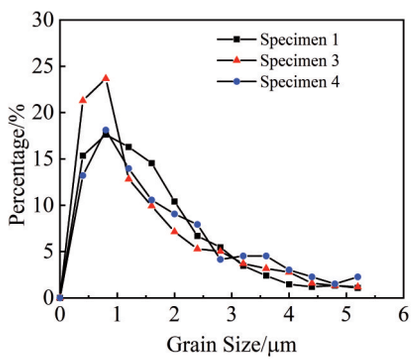

Fig.7 Grain size distribution of specimens 1, 3, and 4

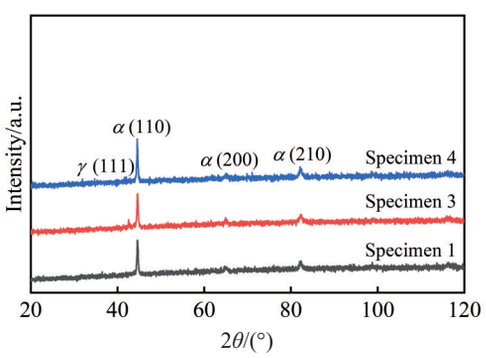

Fig.8 XRD patterns of deposited metals of specimens 1, 3, and 4

at austenite grain boundaries, reducing their grain boundary energy and delaying the nucleation of PF. This results in the decrease in temperature at which austenite transformation begins and proeutectoid ferrite starts to precipitate from austenite during continuous cooling, thereby expanding the austenite phase region and enhancing the stability of austenite. Simultaneously, the solid solution of REEs increases the shear resistance of the martensite transformation and lowers the starting temperature of martensitic transformation. Therefore, the retained austenite content is higher in the deposited metals of specimens 3 and 4, which contain appropriate and excessive amounts of REEs, compared to specimen 1. During impact deformation, the retained austenite undergoes a transformation-induced plasticity (TRIP) effect[23], enhancing the plastic deformation capacity. The formed martensite hard-phase particles can serve as a secondary-phase interface, thereby facilitating the formation of dimples and increasing the crack propagation energy during impact. As the amount of REEs addition increases, the retained austenite content in the deposited metal first increases and then decreases. There is a competitive relationship between the toughening effect of the austenite ductile phase and the embrittlement effect of the martensite brittle phase in the M-A constituents, which is consistent with the overall improvement in low-temperature impact toughness plateau, followed by a subsequent rise and then decline.

Regarding the existence and distribution of REEs in steel, some scholars have pointed out that Ce has a very strong segregation tendency at grain boundaries, significantly higher than that of elements such as S, P, and B. When a small amount of REEs is added to steel, it preferentially forms rare earth inclusions, and the amount of REEs present in solid solution is relatively small[20]. Therefore, this study uses EDS to analyze grain boundaries and determine the influence of REEs content on the microstructure and properties of the deposited metal of 1000 MPa grade high-strength steel.

The grain boundary precipitates of specimens 3 and 4 were scanned using EDS, as shown in Fig.10 and Table 8. When the REEs content is low, the segregated components include alloy elements such as Ni, Mn, and Cr. REEs do not accumulate at the grain boundaries but form complex rare earth inclusions

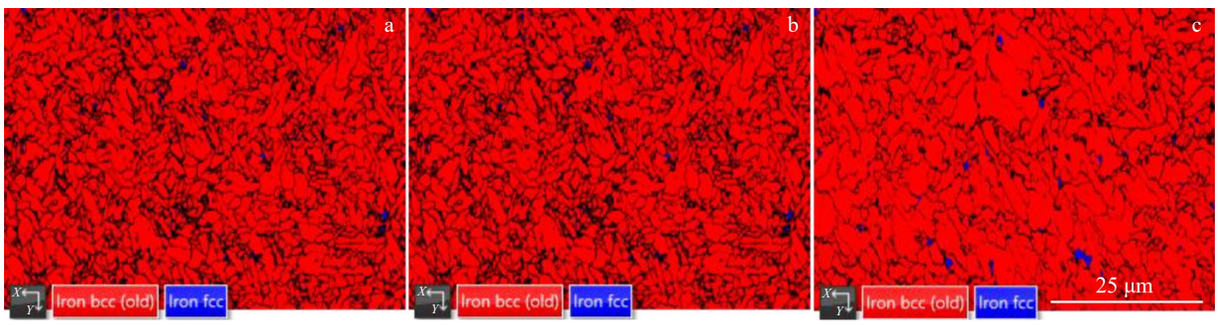

Fig.9 EBSD maps of deposited metal of specimen 1 (a), specimen 3 (b), and specimen 4 (c)

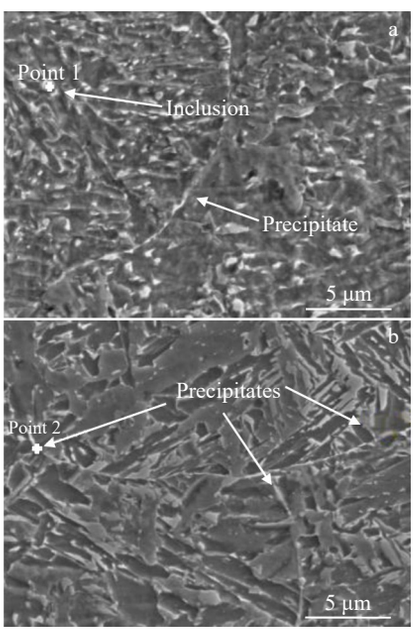

Fig.10 SEM images of grain boundary precipitates: (a) specimen 3; (b) specimen 4

Table 8 EDS results of points marked in Fig.10 (wt%)

Point	S	Al	Ti	Cr	Mn	Ni	Ce
1	0.34	7.72	5.13	0.83	4.80	2.73	0.19
2	7.16	-	-	14.68	7.75	53.51	8.57

within the grains. Fig. 10b indicates that as more REEs are added, REEs begin to precipitate and significantly segregate at the grain boundaries. Scanning multiple precipitates on the impact fracture surface of specimen 4 reveals the presence of REEs, further confirming the phenomenon of significant REEs segregation. According to the composition of precipitates listed in Table 9, excessive REEs can form composite segregation and brittle phases with impurity elements such as S at the grain boundaries, which may become crack sources or crack propagation paths, thus increasing the crack sensitivity and reducing toughness of the deposited metal.

3.4 Inclusion analysis

In HSLA steel, inclusion modification is an effective method to increase the amount of AF. Li et al[24] have proposed

Table 9 Composition of grain boundary precipitates (wt%)

Cr	Mn	Ni	S	Ce
12.73	7.10	52.40	3.83	20.03

that in HSLA steel, inclusions, with a core mainly composed of MnS and other non-crystalline phases, a size of 0.5–0.8 μm, a volume fraction of 36vol%, a surface enriched with a 10–20 nm TiO thin layer, and a spherical shape, can definitely promote the nucleation of AF. In this study, observations were made on inclusions with various sizes in the deposited metal of 1000 MPa grade high-strength steel before and after REEs treatment. SEM images and corresponding EDS element distribution mappings of the inclusions are shown in Fig. 11. From Fig. 10a and 10b, it can be observed that large-sized inclusions are regularly round, and their composition consists of oxides of Mn, Ti, Si, and Al. The distribution of various metal elements in the inclusions is uniform. In Fig. 11a, Si content is relatively low (0.19wt%) and is present at the center of the inclusion. While in Fig. 11b, Si content is higher (0.39wt%) and is mainly distributed on the outer side of the inclusion. From Fig. 11c, it can be seen that small-sized inclusions are REEs inclusions, and two inclusions grow in parallel with different composition. The larger one consists of a small amount of REEs, Mn, Ti, Al, and O, with REEs distributed in the innermost layer, surrounded by alloy elements. Mn and Ti are located in the middle layer, and Al presents in both the middle and outer layers. All three layers are oxides, as schematically shown in Fig.12. The smaller one mainly consists of oxides of Mn, Ti, and Al.

According to the principle of minimum mismatch degree[25], the mismatch degree between composite REEs inclusions and both α-Fe and γ-Fe is less than 12%. Therefore, they can promote the nucleation of AF and austenite on certain crystal plane families, inhibit the nucleation and growth of non-equiaxed ferrite, and the fine and dispersed REEs inclusions can also provide more nucleation sites, pin grain boundaries down, and refine grains. By scanning the crack initiation zone, crack propagation zone, and final fracture zone of the impact fracture surface of the deposited metal of 1000 MPa grade high-strength steel added with REEs, as shown in Fig. 13, it can be found that oxides mainly composed of Mn, Cr, Ni, and Al exist in each dimple in the initiation zone, and no REEs are

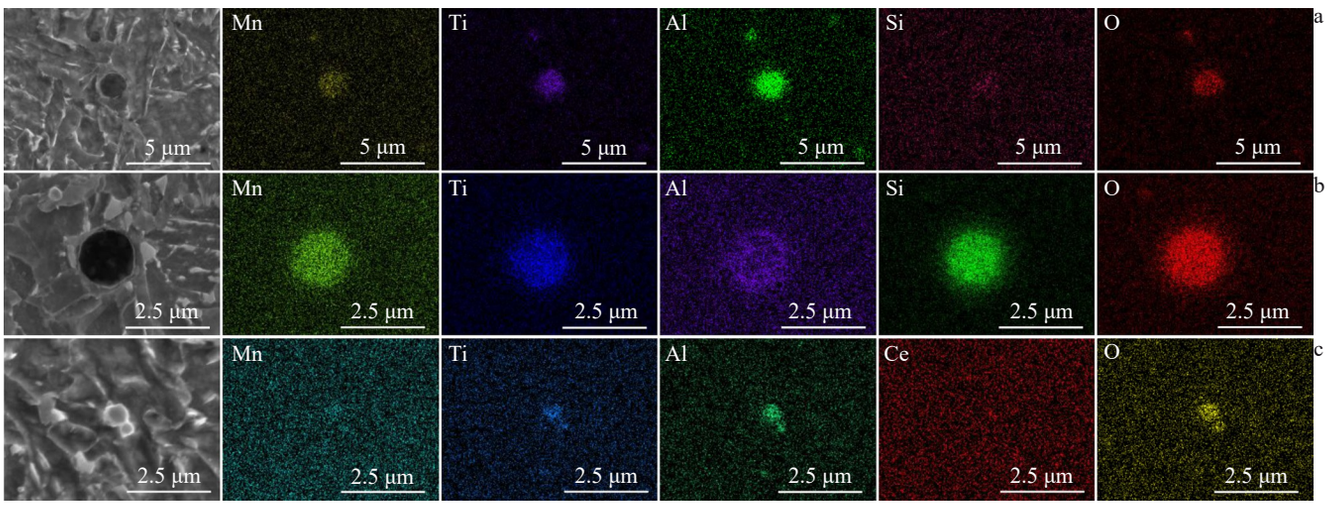

Fig.11 SEM images and corresponding EDS element distribution of large-sized (a–b) and small-sized (c) inclusions

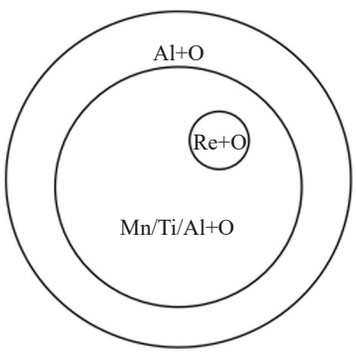

Fig.12 Schematic diagram of REEs inclusions

detected. These brittle inclusions become the sources of crack initiation during the impact process. In the crack propagation zone and the final fracture zone, it can be found that REEs begin to exist with large quantities in both the inclusions and the matrix, proving that REEs inclusions have stronger bonding ability with the matrix compared to common brittle oxide inclusions such as Al_2O_3, and are less prone to causing stress concentration. However, as the stress continues to increase, they can also become paths for crack propagation.

To investigate the influence of REEs content on inclusions in the deposited metal of 1000 MPa grade high-strength steel, metallographic specimens of deposited metal with 0, 2, and 4 parts of REEs addition after grinding and polishing were analyzed under an OM at 1000× magnification. For each specimen, 100 random views were selected, and validity was determined according to the standard test method specified in GB/T 18876.1-2002 of *Standard Test Method for Determining Metallographic Structure, Inclusion Content, and Grade in Steel and Other Metals-Part 1: Image Analysis and Stereological Determination of Inclusion or Second-Phase Structure Content in Steel and Other Metals*. At the same time, SEM observations were conducted on the inclusions and the impact fracture surface of each deposited metal, and the results are shown in Fig.14. The average sizes of specimens 1, 3, and 4 are 0.80, 0.77, and 0.79 μm, respectively. The deposited metal with 2 parts of REEs addition has the highest

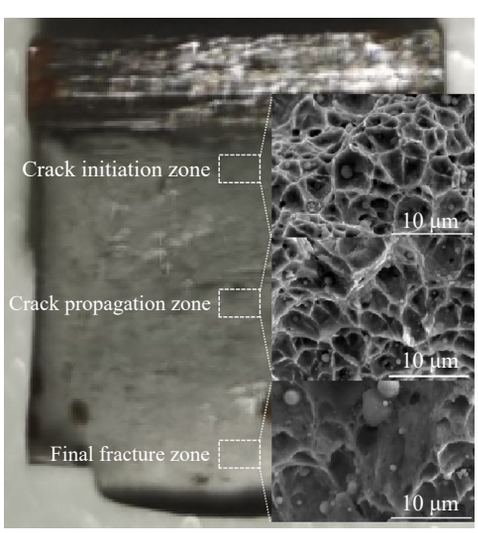

Fig.13 SEM images of impact fracture surfaces in different regions

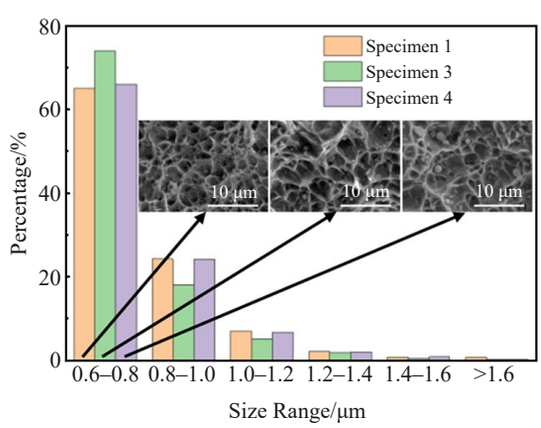

Fig.14 Relationship between inclusion size distribution in deposited metal of 1000 MPa grade high-strength steel and morphology of inclusions on impact fracture surface

Table 10 Relationship between correlation coefficient *r* and inclusion sizes

Inclusion size/μm	0.6–0.8	0.8–1.0	1.0–1.2	1.2–1.4	1.4–1.6	>1.6
Correlation coefficient, *r*	0.802	−0.745	−0.867	−0.952	−0.439	−0.938

proportion of inclusions with sizes of 0.6–0.8 μm, while the proportion of larger-sized inclusions is lower. The correlation coefficient *r* between the proportion of inclusions with various sizes and the impact toughness at −60 °C is calculated using Eq. (1), and the results are shown in Table 10, in which the average value of correlation coefficient *r* is −0.860. It can be inferred that inclusions with sizes ranging from 0.6 μm to 0.8 μm have a highly positive correlation with impact toughness at −60 °C. Inclusions larger than 0.8 μm and the average size are negatively correlated with impact performance, indicating that small-sized inclusions (0.6–0.8 μm) have a positive effect on improving low-temperature impact toughness. As the amount of REEs addition increases, the size of inclusions increases, leading to segregation of REEs. The increased size and accumulation of inclusions at dimples become crack sources, deteriorating performance, and exerting a negative effect.

$$r(X,Y)=\frac{\mathrm{Cov}(X,Y)}{\sqrt{\mathrm{Var}[X]\,\mathrm{Var}[Y]}} \quad (1)$$

where X refers to grain size; Y refers to impact energy; Cov(X, Y) represents the covariance between X and Y; Var[X] denotes the variance of X; Var[Y] denotes the variance of Y.

4 Conclusions

1) By optimizing the submerged arc welding material for 1000 MPa grade high-strength steel through the addition of REEs, excellent welding workability can be achieved in experiments. The overall mechanical properties of the deposited metal can be enhanced with an appropriate amount of REEs addition. As the amount of REEs added increases, the mechanical properties first increase and then decrease. Specifically, the tensile strength improves from 935 MPa to 960 MPa when 2 parts of REEs are added, but it drops to 885 MPa with excessive addition. The yield strength increases by 8.5% to 17.2%. And the impact energy at −40 °C increases by 8.5% to 24.3%, while it increases by 15.6% to 42.2% at −60 °C.

2) When an appropriate amount of REEs is transitioned into the deposited metal, it leads to grain refinement and an increase in AF and retained austenite content, thereby significantly improving the low-temperature impact toughness. However, as the addition amount increases, REEs segregation occurs, leading to deterioration of grain boundaries, the formation of coarse grains, and a decrease in retained austenite content, and resulting in a reduction in low-temperature impact toughness. Experiments have determined that the best strength-toughness match for the deposited metal is achieved when 2 parts of REEs are added.

3) The appropriate addition of REEs can modify the inclusions, and produce fine and dispersed composite inclusions that bond better with the matrix. Rare earth inclusions can strengthen the material by inducing the formation of AF nuclei and refining ferrite grains. After adding REEs, the average size of the inclusions decreases, and the proportion of inclusions with sizes ranging from 0.6 μm to 0.8 μm increases, which can enhance the impact toughness of the deposited metal. Inclusions larger than 0.8 μm, on the other hand, can reduce its impact toughness.

References

1 Li Xiaozhu, Chen Zhijun, Fan Xiaochao *et al. Renewable and Sustainable Energy Reviews*[J], 2018, 82(Part 1): 232

2 Pérez-Díaz J I, Chazarra M, García-González J *et al*. *Renewable and Sustainable Energy Reviews*[J], 2015, 44: 767

3 Horikawa K, Watanabe N. *Welding in the World: Journal of the International*[J], 2008, 52: 3

4 Hara N, Sato M. *Conference on High Strength Steels for Hydropower Plants*[C]. Takasaki: ISIJ, 2009

5 Kippenhan N, Gschneidner K. *Rare-Earth Metals in Steels*[R]. Ames: Iowa State University of Science and Technology, Rare-Earth Information Center, 1970

6 Preinfalk C, Morteani G. *Lanthanides, Tantalum and Niobium: Mineralogy, Geochemistry, Characteristics of Primary Ore Deposits, Prospecting, Processing and Applications*[C]. Berlin: Springer, 1989: 359

7 Li Chunlong. *Chinese Rare Earths*[J], 2013, 34(3): 78 (in Chinese)

8 Wang Lifeng, Liu Fengde, Zhang Hong *et al*. *Journal of Mechanical Engineering*[J], 2016, 52(22): 70

9 Meng Xianghai, Wang Wei, Bi Sheng *et al*. *Iron and Vanadium Titanium*[J], 2022, 43(2): 146 (in Chinese)

10 Zang Ruoyu, Li Jing, Huang Fei. *Nonferrous Metals Science and Engineering*[J], 2024,15(3):449 (in Chinese)

11 Gao Huimin, Fang Qi, Sun Wei. *World Nonferrous Metals*[J], 2017(11): 267 (in Chinese)

12 Qin Mu, Yang Xiong, Yang Weiyu. *Science & Technology of Baotou Steel*[J], 2020, 46(2): 52 (in Chinese)

13 Feng Wei, Yu Tingxiang, Xu Kai *et al*. *Welding & Joining*[J], 2023(11): 6

14 Zhang Min, Yao Chengwu, Li Jihong *et al*. *Transactions of the China Welding Institution*[J], 2006(10): 29 (in Chinese)

15 Ding Guangzhu, Guo Weiyun, Wang Shunxing *et al*. *Welding Technology*[J], 2020, 49(5): 90

16 Sharma L, Chhibber R. *Ceramics International*[J], 2019, 45(2): 1569

17 Sharma L, Chhibber R. *Ceramics International*[J], 2020, 46(2): 1419

18 Zhang Wenye. *Welding Metallurgy*[M]. Beijing: China Machine

Press, 1993 (in Chinese)
19 He Lei, Wang Renfu, Cheng Yingjin *et al*. *Transactions of the China Welding Institution*[J], 2023, 44(5): 7 (in Chinese)
20 Geng Ruming. *Effect of Cerium on Microstructures and Mechanical Properties in Heat-Affected Zone of High-Strength Steel Applied to Construction Machinery*[D], Beijing: University of Science and Technology Beijing, 2022 (in Chinese)
21 Wang Longmei. *Application of Rare Earth Elements in Low Alloy and Alloy Steels*[M]. Beijing: Metallurgical Industry Press, 2016
22 Qu Wei, Ren Huiping, Jin Zili *et al. Rare Metal Materials and Engineering*[J], 2018, 47(7): 2087 (in Chinese)
23 Soleimani M, Kalhor A, Mirzadeh H. *Materials Science & Engineering A*[J], 2020, 795: 140023
24 Li Zhuoxin, Zhang Tianli, Kim H J. *Materials China*[J], 2012, 31(1): 50 (in Chinese)
25 Brammfitt B L. *Metallurgical Transactions*[J], 1970, 1: 1987

稀土元素对1000 MPa级高强钢埋弧焊熔敷金属组织性能的影响

李春剑[1,2]，徐　锴[1,2]，冯　伟[1]，宋昌洪[1]，张庆素[1]，郝乾宇[1]，郑勇强[1]，郭旭超[3]
(1. 哈尔滨威尔焊接有限责任公司，黑龙江 哈尔滨 150000)
(2. 中国机械总院集团 哈尔滨焊接研究所有限公司，黑龙江 哈尔滨 150028)
(3. 苏州天兵科技有限公司，江苏 苏州 215004)

摘　要：通过在焊材中添加稀土元素优化熔敷金属性能，并利用光学显微镜、扫描电子显微镜、能谱仪、X射线衍射仪等仪器，结合Matlab、Image-Pro Plus、CHANNEL5等软件研究了稀土元素添加量对1000 MPa级高强钢熔敷金属强韧性及夹杂物的影响机理。结果表明，稀土元素的添加提高了焊材的焊接工艺性。随稀土元素的添加，熔敷金属抗拉伸强度从935 MPa提高到960 MPa，继续添加则导致了抗拉伸强度下降，而屈服强度持续提高8.5%~17.2%。适量稀土元素的添加使熔敷金属针状铁素体及残余奥氏体含量提高、晶粒细化，致使−40 ℃冲击功增加8.5%~24.3%、−60 ℃冲击功增加15.6%~42.2%。此外，适当添加稀土元素还能改性夹杂物，能够生成细小弥散且与基体结合更好的复合夹杂物，通过多种机制优化熔敷金属性能。因此，适量添加稀土元素可大幅提升1000 MPa级高强钢熔敷金属性能，提升熔敷金属的高强韧性匹配，满足水电用高强钢的使用需求。

关键词：1000 MPa级高强钢；熔敷金属；埋弧焊；稀土元素；夹杂物

作者简介：李春剑，男，1996年生，硕士生，中国机械总院集团哈尔滨焊接研究所有限公司，黑龙江 哈尔滨 150028，E-mail：chumjane@126.com